CrystEngComm

Accepted Manuscript

ROYAL SOCIETY OF CHEMISTRY

www.rsc.org/crystengcomm

The effects of precursors on morphology and microstructure of potassium sodium niobate nanorods synthesized by molten salt synthesis

Luying Luo,[a] Chao Chen,[a] Hang Luo,[a] Ye Zhang,[a,b] Kechao Zhou,[a] and Dou Zhang*[a]

[a]State Key Laboratory of Powder Metallurgy, Central South University, Changsha, Hunan 410083, China.

[b]School of Metallurgy and Materials, University of Birmingham, Edgbaston, Birmingham B15 2TT, UK

Abstract:

(K, Na)NbO_3 (KNN) nanorods were fabricated by molten salt synthesis (MSS) through Nb_2O_5 and $K_2Nb_4O_{11}$ precursors, respectively. The phase and composition of KNN nanorods were characterized by X-ray diffraction and inductively coupled plasma spectrometry. The microstructure and crystal growth orientation of the KNN nanorods were investigated by scanning electron microscopy and transmission electron microscopy. All the products were proved to be single crystal. KNN nanorods produced by Nb_2O_5 precursors were short and agglomerate with a aspect ratio of 6:1, while that produced by $K_2Nb_4O_{11}$ precursors showed an aspect ratio of nearly 15:1, which could be utilized for bio-sensing and energy-harvesting micro-devices. It was proposed that the shortness and agglomeration of KNN nanorods produced from Nb_2O_5 precursors were originated from the layered structures of the pristine precursors in fabricating Nb_2O_5. The KNN nanorods produced from $K_2Nb_4O_{11}$ showed a preferable stoichiometry with K/Na ratio closer to 50:50 than that produced from Nb_2O_5, which was attributed to the ability of $K_2Nb_4O_{11}$ nanorods for maintaining K content in the reaction process. In addition, the piezoelectric properties of individual KNN nanorod produced from Nb_2O_5 and $K_2Nb_4O_{11}$ precursors were confirmed by piezoresponse force microscopy, as the converse piezoelectric coefficient d_{33}* were calculated to be 95 pm/V and 201 pm/V, respectively. The results obtained in this work would provide a valuable guide for further improving the MSS process to synthesize KNN nanorods with large aspect ratio and high performance.

Keywords: KNN, piezoelectric, lead-free, nanorods, molten salt synthesis

1. Introduction

Nanoscale one-dimensional (1-D) piezoelectric materials, including nanotubes[1] and nanorods[2] and nanowires[3, 4], have attracted intensive attention in recent years for their novel shape-dependent properties[5-7] and their wide applications in energy harvesting[8-10] such as micro-electromechanical system[11] and nano-electromechanical system[12, 13]. The vast majority of piezoelectric materials are based on $PbZr_{1-x}Ti_xO_3$ for their superior performance[14, 15], however, their high concentrations of lead compromised its usefulness in many fields with the purpose of protecting human health as well as environment. Therefore, enormous efforts have been devoted to the development of lead-free counterparts such as $BaTiO_3$[13, 16], $Bi_{0.5}Na_{0.5}TiO_3$[17], (K, Na)NbO_3 (KNN)[18], etc. 1-D perovskite structures of those lead-free piezoelectric materials could be more efficiently integrated in devices. KNN, which is a combination of ferroelectrics $KNbO_3$ and anti-ferroelectrics $NaNbO_3$, was reported to have the best piezoelectric properties near the morphology phase boundary when K/Na≈1 in KNN ceramics[19]. And for its advantages of high piezoelectric constant and high curie temperature, KNN has been one of the most investigated lead-free piezoelectric systems in recent years[20]. Several routes have been used to synthesize 1-D materials in this system, such as sol-gel synthesis[21], hydrothermal synthesis[22, 23] and molten salt synthesis (MSS)[24]. MSS is a rapid and large-scale process for ternary complex oxides with 1-D nanostructures. The molten flux increases the diffusivity of the species (up to 10 orders of magnitude), leading to a reduction of the reaction time and temperature, as well as the loss of volatile species[25].

Various precursors were used to synthesize KNN nanorods[26]. Nb_2O_5, which was transformed from KNb_3O_8, was extensively used as a precursor to obtain KNN 1-D nanostructures[27, 28]. $K_2Nb_4O_{11}$ was also reported as precursors in fabricating KNN[29]. However, the distinctions of KNN nanorods produced by different precursors have been overlooked. Herein, this study aims to compare the microstructures, morphologies, reaction mechanisms and piezoelectric properties of KNN nanorods produced from Nb_2O_5 and $K_2Nb_4O_{11}$ precursors, in order to provide a valuable guide

for understanding effects of using different precursors on synthesizing KNN nanorods. Nb_2O_5 nanorods were obtained step by step from rod-like KNb_3O_8 , while $K_2Nb_4O_{11}$ nanorods were obtained directly after the raw materials were heated at 1000 °C for 3 h. The effects of the two precursors on the morphologies and compositions of final KNN nanorods were investigated. The phase transition and the main factors influencing the structures and compositions of the KNN nanorods were discussed.

2. Experimental

K_2CO_3 (Sinopharm, China, ≥99.0%), Nb_2O_5 (Sinopharm, China, 99.99%) and KCl (Sinopharm, China, ≥99.5%) were used as raw materials and mixed in ethanol according to a molar ratio of 0.1:3:30, in order to synthesize the rod-like Nb_2O_5 precursors. The mixture was heated at 5 °C/min and dwelled at 800 °C for 3 h. After air cooling and washing with de-ionized water for several times, the rod-like KNb_3O_8 was obtained as pristine precursors. Intermediate precursors $H_3ONb_3O_8$ was then synthesized by adding 1 g of KNb_3O_8 to 400 ml HNO_3 (2 M) and stirring for 48 h at 90 °C. After drying in the oven and heating at 600 °C for 1 h to lose H_2O, Nb_2O_5 rod-like precursors was obtained.

Rod-like $K_2Nb_4O_{11}$ precursors were also synthesized by K_2CO_3, Nb_2O_5 and KCl. The raw materials were mixed in ethanol with a molar ratio of 1:3:30. Then the mixture was heated at a rate of 5 °C/min and dwelled at 1000 °C for 3 h. After air cooling and washing with de-ionized water for several times to remove excessive KCl salt, the rod-like $K_2Nb_4O_{11}$ was obtained.

The processes of synthesizing KNN nanorods by the two different precursors were similar using MSS. Na_2CO_3 (Sinopharm, China, ≥99.8%), K_2CO_3 and the precursors were mixed by corresponding molar ratio according to final product $(K_{0.5}Na_{0.5})NbO_3$. Considering the volatilization of alkali metal ions during sintering, 10 wt% over-mass of alkali metal carbonate were added. KCl powders were added in an equal weight to the sum of other reactants. All the reactants were heated at 850 °C for 10 mins with a heating rate of 5 °C/min. After cooling to the room temperature, the excessive KCl salt

were removed by washing the products with de-ionized water for several times. The KNN nanorods obtained from Nb_2O_5 and $K_2Nb_4O_{11}$ precursors were marked as KNN1 and KNN2, respectively.

The phase structures of the samples were characterized by X-ray diffraction patterns (XRD, D/max 2550PC) with Cu-Kα radiation, and the microstructures of the products were observed using scanning electron microscopy (SEM, Quanta-200). The compositions of the products were analyzed using inductively coupled plasma (ICP, PerkinElmer optima 5300 DC) spectrometry. Transmission electron microscopy (TEM) observations with selected area electron diffraction (SAED) patterns and the high-resolution transmission electron microscopy (HRTEM) were performed on a transmission electron microscope (JEM-2100F), while the samples were prepared by placing a drop of dilute alcohol to disperse the nanorods on a covered copper grid.

The piezoelectric properties of KNN1 and KNN2 nanorods were measured using piezoresponse force microscopy (PFM) mode of an atomic force microscopy (NanoManTM VS) with a conductive Pt/Ir-coated Si cantilever (SCM-PIT), which has a spring constant of 2.8 N/m and a free resonance frequency of 75 kHz. The nanorods were first dispersed on a Pt-electroded Si wafer, the tip of cantilever was then held at one point of an individual nanorod. The piezoresponse measurements were then obtained by applying a direct current (DC) voltage from -10 V to 10 V superimposed on an alternating current modulation voltage with a frequency of 41 kHz, away from the contact resonance. The displacements along the vertical direction of KNN1 and KNN2 nanorods were obtained and the converse piezoelectric coefficient d_{33}* was calculated.

3.Results and Discussions

(a) Synthesis of KNN1 via precursors of Nb_2O_5 nanorods.

For the present molten salt synthesis, the key point is to obtain high-aspect-ratio precursors, which then act as templates for the formation of final products. Therefore, it is necessary to consider the first step as the most critical step in the whole

synthesis[30]. Fig. 1a shows the XRD patterns of KNb_3O_8 in the 2θ range of 20~60°. All diffraction peaks can be assigned to an orthorhombic phase of KNb_3O_8 (PDF#75-2182), identifying pure KNb_3O_8 phase with no trace of any second phase. The ion exchanging characteristic of KNb_3O_8 was confirmed by its ability to exchange the K ion with the H_3O ion, leading to $H_3ONb_3O_8$ compound. The XRD pattern of $H_3ONb_3O_8$, as shown in Fig. 1b, demonstrated an orthorhombic structure (PDF#44-0672) without any detectable secondary phases. After $H_3ONb_3O_8$ nanorods dried in the oven and heated at 600 °C, the final precursors of Nb_2O_5 nanorods were obtained. XRD pattern, as shown in Fig. 1c, proves that the final precursors were pure monoclinic phase of Nb_2O_5, according to PDF#43-1042.

Fig. 2 shows the SEM images and the structural schematics of KNb_3O_8, $H_3ONb_3O_8$, and Nb_2O_5 in each step, respectively. As shown in Fig. 2a, the KNb_3O_8 nanorods were 2~25 μm long (average 10 μm) and 0.2~1 μm wide (average 0.3 μm), with an aspect ratio of nearly 33:1. The KNb_3O_8 nanorods were straight and had flat and smooth surfaces. However, after stirring in HNO_3 solution (2 M) for 24 h and calcining, the morphologies of $H_3ONb_3O_8$ and Nb_2O_5 nanorods gradually became much clutter and shorter compared to KNb_3O_8 precursors, as shown in Fig. 2c and Fig. 2e, indicating the processes and reactions had certain influences on the morphology. KNb_3O_8 was reported to be a layered structure and could be characterized as a stacking of $–Nb_3O_8–$ sheets consisting of corner-sharing and edge-sharing NbO_6 octahedra, while K atoms were located between the $–Nb_3O_8–$ sheets[27], as shown in Fig. 2b. In each sheet, three NbO_6 octahedra connected with sharing corners and edges along the b-axis. During stirring in HNO_3 solution, an ion-exchange of K^+ ions by H_3O^+ ions would happened according to the reaction[31]:

$$KNb_3O_8 \xleftarrow[K^+]{H_3O^+} H_3ONb_3O_8 \qquad (1)$$

During the reaction, $–Nb_3O_8–$ sheets did not change. The H_3O^+ ions in $H_3ONb_3O_8$ were located at approximately the same places as those of K^+ ions in KNb_3O_8, so the layered structure of $H_3ONb_3O_8$, as shown in Fig. 2d, was similar to that of KNb_3O_8. The exchange reaction was reversible and afterwards, $H_3ONb_3O_8$ nanorods were

heated to lose H_2O in order to get Nb_2O_5 precursors. Actually, KNb_3O_8 and $H_3ONb_3O_8$ could also be used to produce KNN directly as reported by L. Li et al[28]. However, the layered structures of KNb_3O_8 and $H_3ONb_3O_8$ nanorods, which might be easier to be decomposed and damaged by the transportation of K^+ in the molten salt environment, were instable compared with Nb_2O_5 nanorods, during the reaction process of producing KNN. The final KNN particles would be small cubic-like instead of rod-like after the destruction of the layered structures. Therefore it is necessary to use Nb_2O_5 nanorods, which have more stable thermodynamic structure as precursors for producing KNN.

L. Li et al. reported that two steps were needed to obtain Nb_2O_5 with the following reactions[28]:

$$H_3ONb_3O_8 \rightarrow HNb_3O_8 + H_2O\uparrow \rightarrow \frac{3}{2}Nb_2O_5 + \frac{3}{2}H_2O\uparrow \qquad (2)$$

When H_3O^+ dehydrated to H^+, the neighboring sheets became closer. Furthermore, H^+ disengaged from $–Nb_3O_8–$ sheets, and the sheets finally connected by sharing the corner of NbO_6 octahedra. So Nb_2O_5 precursors could also be described as the units of identical NbO_6 octahedra with corner and edge-sharing, as shown in Fig. 2f. The reactions involved lots of breaking, re-arranging, and forming of bonds. The nanorods maybe easier to tear apart and break up due to the layered structures during the ion-exchanging and dehydration reactions[32].

TEM images shown in Fig. 3 confirmed the single crystallinity of all the nanorods. As shown in Fig. 3a and Fig. 3b, the growth direction of the KNb_3O_8 nanorod was along [011] according to the HRTEM and SEAD patterns. The interplanar spacing observed from HRTEM image was 3.88 Å corresponding to (011) crystal planes of orthorhombic system. Furthermore, the entire KNb_3O_8 nanorod showed a continuous bright contrast, indicating that there was no obvious defect in KNb_3O_8 nanorod. Fig. 3c shows the bright-field TEM image of $H_3ONb_3O_8$ nanorod with a diameter of 140 nm. The SAED pattern (inset of Fig. 3c) along the $[1\bar{1}1]$ direction shown in Fig. 3c indicated that the $H_3ONb_3O_8$ nanorod was structurally uniform with a single crystalline orientation. As shown by HRTEM image of $H_3ONb_3O_8$ nanorod in Fig. 3d,

the lattice planes were (220) and (022) with the interplanar spacing of 4.35 Å and 1.89 Å, respectively. The growth direction was along [011] according to the HRTEM and SEAD patterns. Fig. 3e shows the bright-field TEM image of Nb_2O_5 nanorod, with a diameter of 300 nm. The clear diffraction spots in the SAED pattern (inset of Fig. 3e) indicated the single-crystalline nature, which was further confirmed by the HRTEM observation. The interplanar spacing shown in Fig. 3f was 3.51 Å, corresponding to the (011) crystal planes, which indicated that the growth direction of current Nb_2O_5 nanorod was along [011]. The crystal growth orientations of all the precursors were along [011], confirming the inheritance of structures during the reaction processes. It was proposed that most of the bond-breaking and rebonding had a certain angle to the growth direction according to the structures of the nanorods. That may cause the nanorods easier to break into short and small parts along the growth direction during the reaction processes because of the layered structures, which was also reflected from the morphological observations.

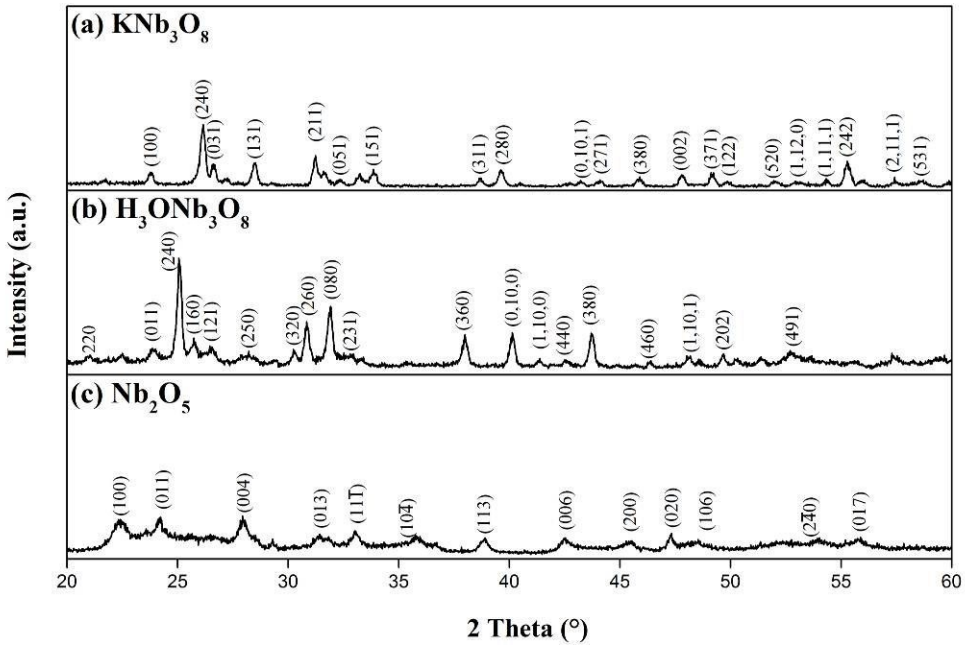

Fig. 1 XRD patterns of (a) KNb_3O_8 nanorods produced by MSS, (b) $H_3ONb_3O_8$ nanorods after stirring the KNb_3O_8 in HNO_3, and (c) Nb_2O_5 nanorods after drying the $H_3ONb_3O_8$ in oven at 600 °C for 1 h.

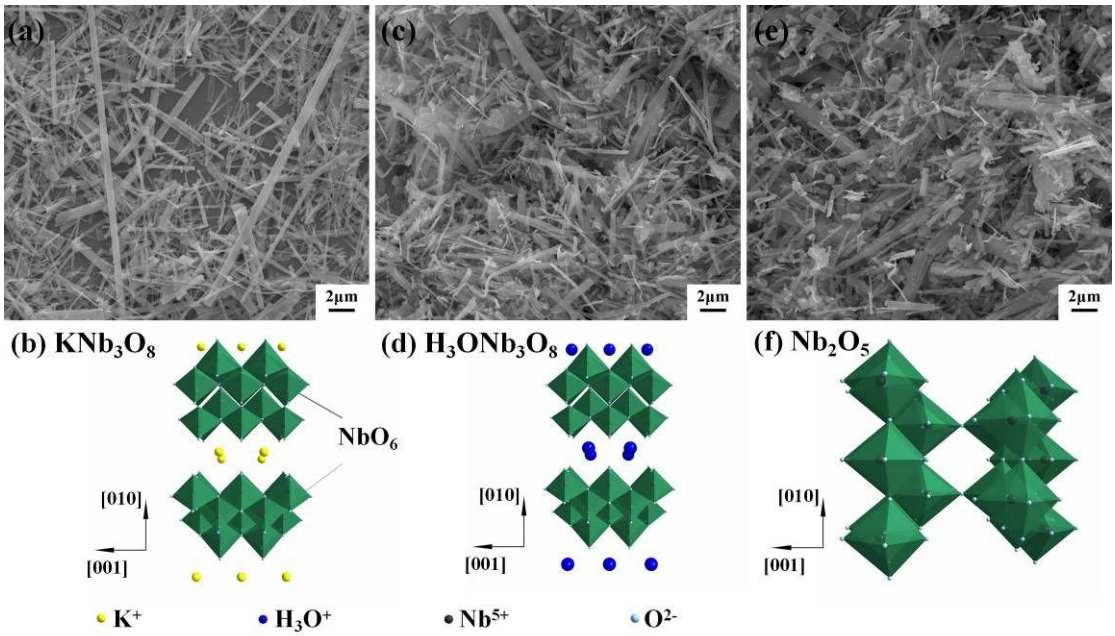

Fig. 2 SEM images of (a) KNb_3O_8 nanorods, (c) $H_3ONb_3O_8$ nanorods, and (e) Nb_2O_5 nanorods and the corresponding schematic structural diagrams of (b) KNb_3O_8, (d) $H_3ONb_3O_8$, and (f) Nb_2O_5, respectively.

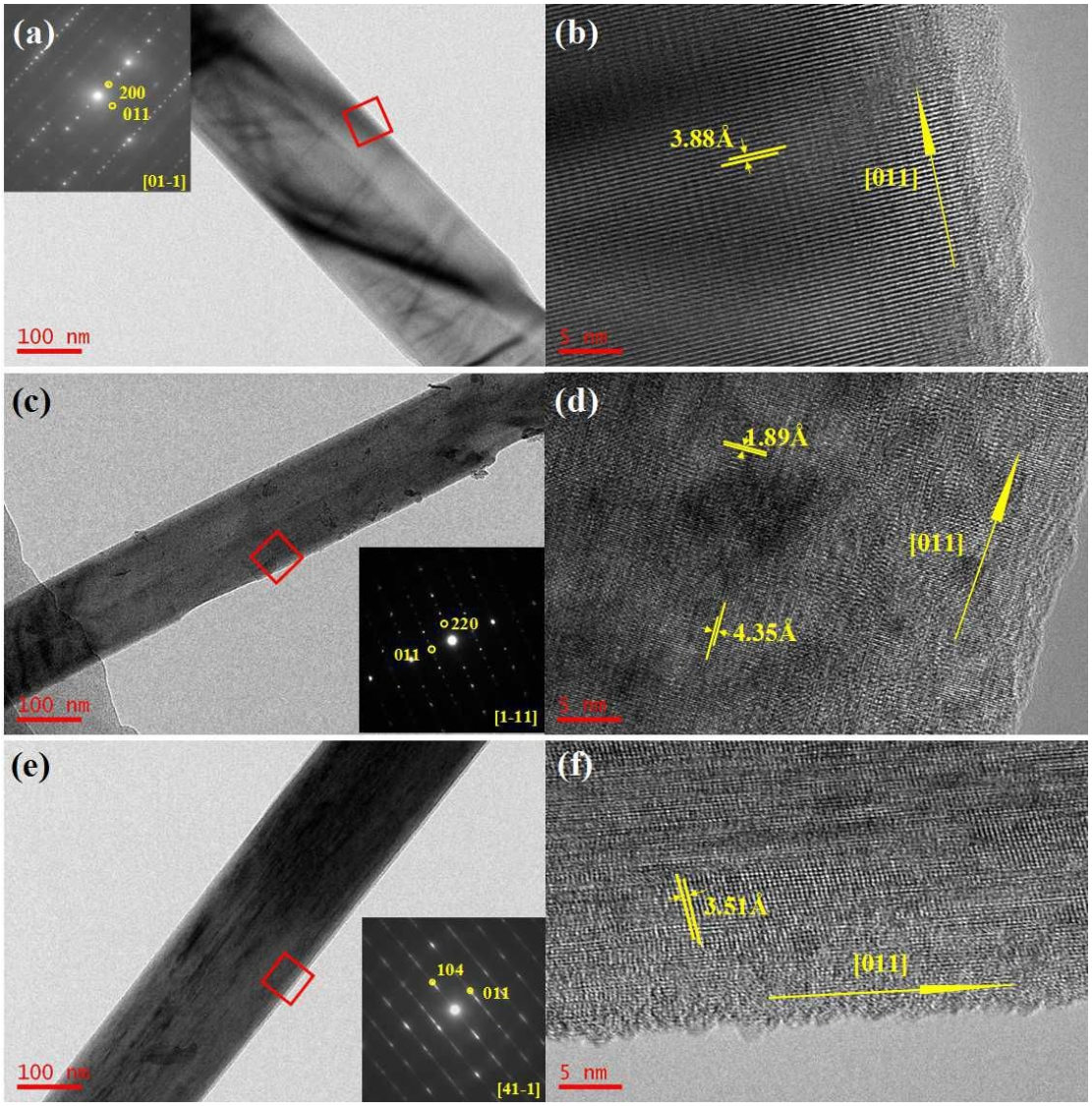

Fig. 3 TEM images of the precursors. (a) Bright-field TEM image of a single KNb_3O_8 nanorod. The inset is the corresponding SAED. (b) HRTEM image of the red square in (a). (c) Bright-field TEM image of a single $H_3ONb_3O_8$ nanorod. The inset is the corresponding SAED. (d) HRTEM image of the red square in (c). (e) Bright-field TEM image of a single Nb_2O_5 nanorod. The inset is the corresponding SAED. (b) HRTEM image of the red square in (e).

Nb_2O_5 nanorods were heated with Na_2CO_3 and K_2CO_3 in KCl molten salts to produce KNN1 and the reaction was considered as follows[33]:

$$2Nb_2O_5 + Na_2CO_3 + K_2CO_3 \rightarrow 4(K_{0.5}Na_{0.5})NbO_3 + 2CO_2\uparrow + O_2\uparrow \qquad (3)$$

Fig. 4a shows the phase structure of KNN1 and matched patterns according to

PDF#71-0946 with an orthorhombic symmetry. Fig. 4b shows the SEM image of KNN1 nanorods with diameters of 0.2~0.8 μm (average 0.5 μm) and lengths of 1~10 μm (average 3 μm). The average aspect ratio was about 6:1. The occurrence of small particles and a rather large distribution range of diameter and length likely attributed to the break-up of previous precursors due to the layered structure and the slight dissolution of Nb_2O_5 nanorods in the molten salts[34]. It is found that the average diameter of nanorods increased and many rods are getting short and bonding together. This may due to higher surface activity of broken Nb_2O_5 precursors, which have smaller particle size and larger specific surface area. The morphology of the obtained KNN1 is not ideal because of the agglomeration.

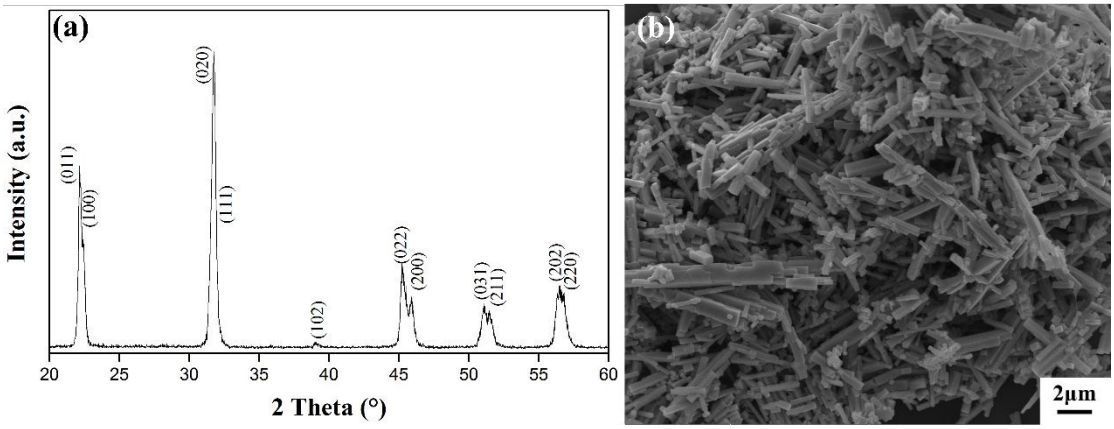

Fig. 4 (a) XRD pattern of KNN1. (b) SEM micrograph of KNN1.

(b) Synthesis of KNN2 via precursors of $K_2Nb_4O_{11}$ nanorods.

The phase structure of $K_2Nb_4O_{11}$ nanorods was detected by XRD and shown in Fig. 5a. The $K_2Nb_4O_{11}$ nanorods showed matched pattern, as indexed by PDF#70-5051 with an orthorhombic symmetry. No trace of any impurity phase was observed. According to the XRD result and related literatures[35], the anions of $K_2Nb_4O_{11}$ had a framework based on the tetragonal bronze structure, and most of the Nb atoms occupied octahedra while the others shared NbO_6 octahedra by corners, located between two NbO_6 octahedra, as shown in Fig. 6d. SEM image gives a good impression on the morphology of $K_2Nb_4O_{11}$ nanorods used as precursors, exhibiting a

very flat, smooth surface, as shown in Fig. 5b. As can be seen, the nanorods were 4~35 μm long (average 25 μm) and 0.15~1 μm wide (average 0.6 μm), giving an aspect ratio of nearly 40:1, which was higher than Nb_2O_5 nanorods reported above. A bright-field TEM image taken from a randomly selected nanorod was presented in Fig. 6a, showing a width of 150 nm. A HRTEM image was shown in Fig. 6b, demonstrating that the $K_2Nb_4O_{11}$ nanorod was single crystalline with a near-perfect crystal structure. The 4.02 Å lattice spacing corresponds to the (001) lattice plane, indicating this nanorod grew along the [001] direction, which was further demonstrated by SAED pattern in Fig. 6c. The SAED pattern along the $[1\bar{3}0]$ direction shown in Fig. 6c indicated that the $K_2Nb_4O_{11}$ nanorod was structurally uniform with a single crystalline orientation and also revealed the growth of the rod was along the [001] direction.

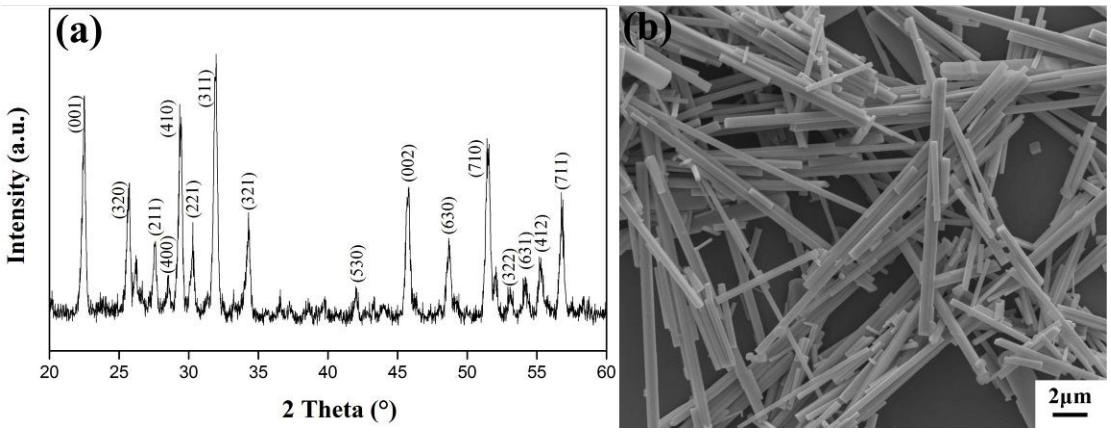

Fig. 5 (a) XRD pattern and (b) SEM micrograph of $K_2Nb_4O_{11}$.

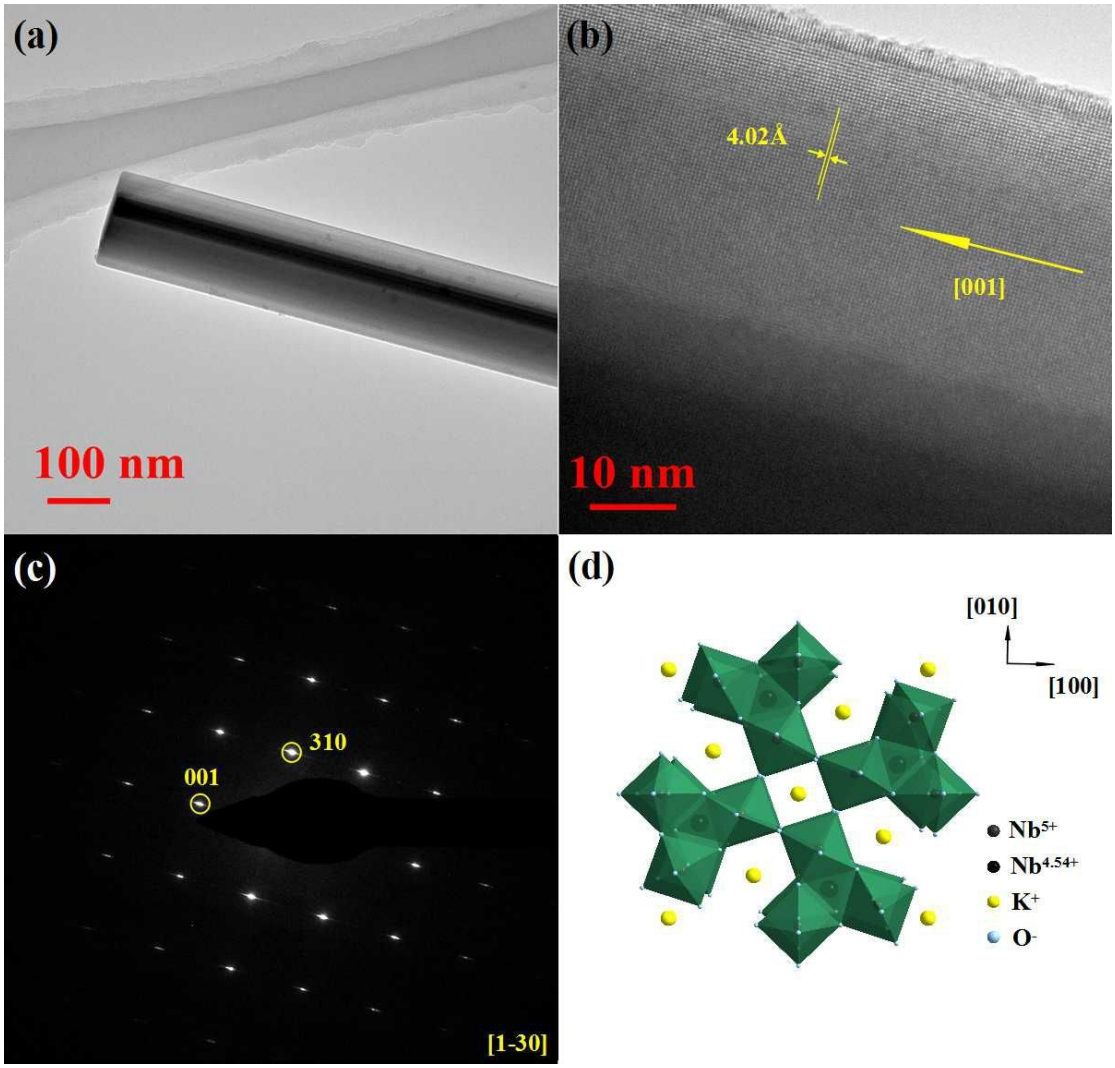

Fig. 6 (a) Bright-field image of an individual $K_2Nb_4O_{11}$ nanorod. (b) HRTEM image from (a). (c) The corresponding SAED pattern of (b) and (d) is the structure schematic diagram of $K_2Nb_4O_{11}$.

$K_2Nb_4O_{11}$ and Na_2CO_3 served as the reactants in KCl molten salt in order to obtain KNN2. The reaction derived as[29]

$$K_2Nb_4O_{11} + Na_2CO_3 \rightarrow 4(K_{0.5}Na_{0.5})NbO_3 + CO_2\uparrow \qquad (4)$$

XRD pattern, shown in Fig. 7a, proved that these KNN2 nanorods were pure orthorhombic phase, corresponding to PDF#71-0946. SEM image of KNN2 was shown in Fig. 7b, nanorods with a width of 0.2~0.8 μm (average 0.6 μm) and a length of 4~25 μm (average 10 μm) were observed, giving an aspect ratio of nearly 15:1. The magnification of all the SEM images in this paper was identical in order to make a

clear comparison. Statistically speaking, KNN2 nanorods obviously had a better aspect ratio on average as compared with KNN1. As can be seen, KNN2 nanorods inherited the morphology of smooth surface and length from the $K_2Nb_4O_{11}$ precursors. Obviously, the obtained KNN2 had the advantage over KNN1 on morphology, due to the smooth surface, aspect ratio and also the dispersion inherited from $K_2Nb_4O_{11}$ nanorods precursors.

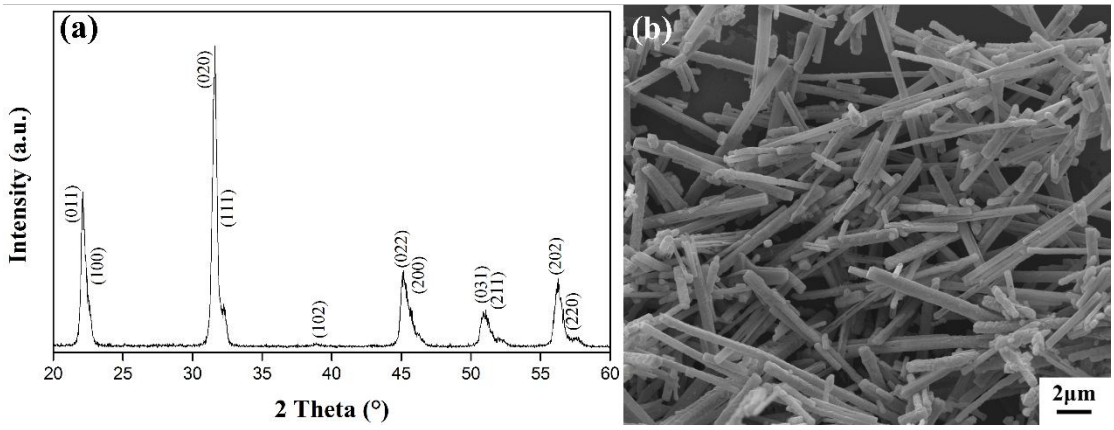

Fig. 7 (a) XRD pattern of KNN2. (b) SEM micrograph of KNN2.

(c) Reaction mechanisms and piezoelectric properties of KNN nanorods synthesized by different precursors.

The KNN nanorods synthesized from the two kinds of precursors showed big difference in the microstructures as well as compositions. In order to explain this phenomenon, the crystal structures of KNN1 and KNN2 were further analyzed. Fig. 8 shows the TEM images of as-synthesized KNN nanorods, in order to get the distinct lattice image, smaller and thinner nanorods were chosen in TEM characterizations. The continuous bright contrast indicated that there were no obvious defects in both of the KNN nanorods. The corresponding SAED patterns were given in the insets of Fig. 8a and Fig. 8c, confirming the single-crystalline nature of the products and also revealing that the growth of the rods was along the [100] direction. The interplanar spacings shown in Fig. 8b and Fig. 8d were 3.96 Å and 3.98 Å, corresponding to the (100) crystal planes.

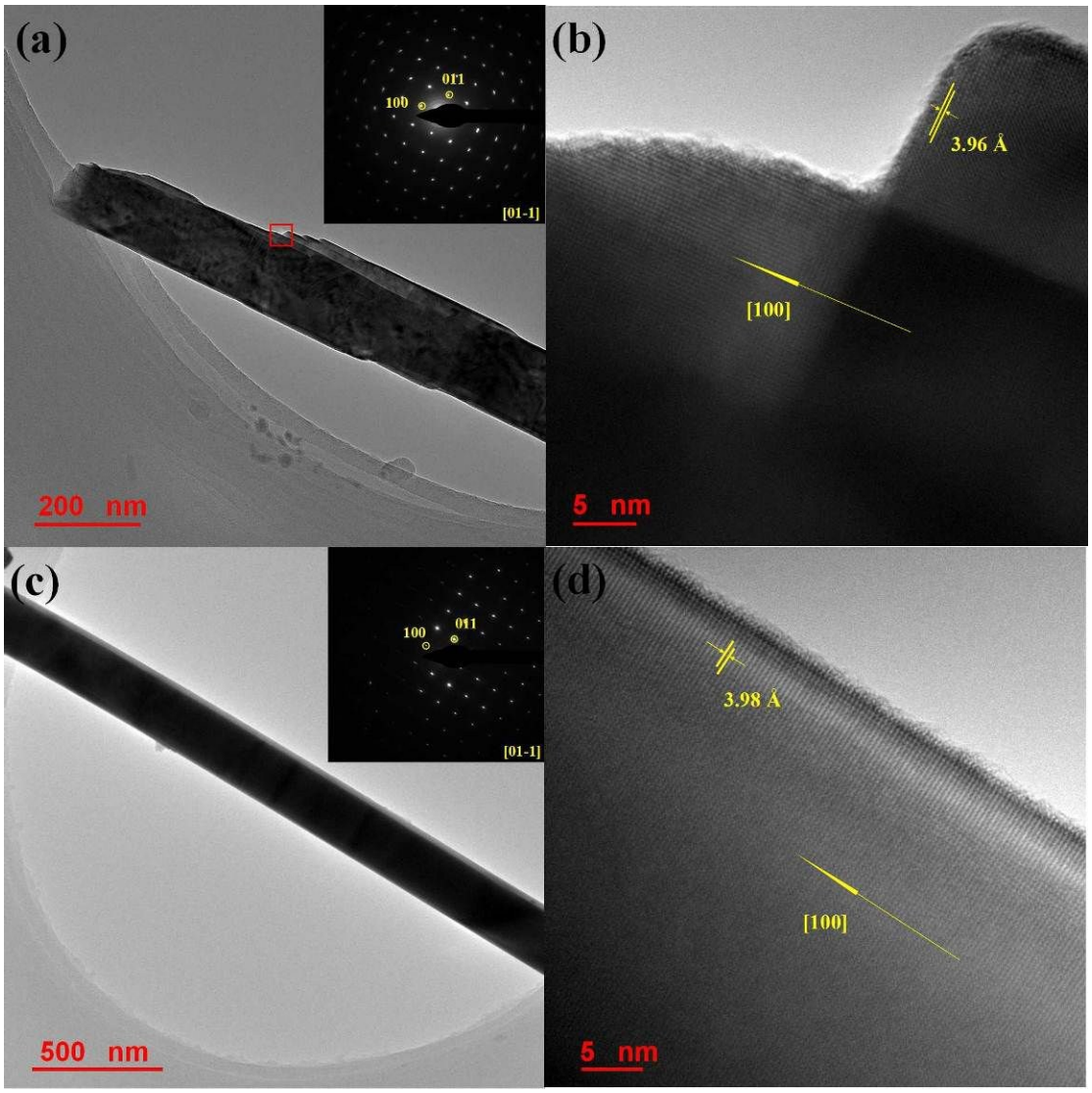

Fig. 8 (a) Bright-field image of an individual KNN1 nanorod. The inset is the corresponding SAED. (b) HRTEM images of the red square in (a). (c) Bright-field image of an individual KNN2 nanorod and the inset is the corresponding SAED. (d) HRTEM image from (c).

For comparison, XRD patterns of both KNN nanorods were shown in Fig. 9. As can be seen in the enlarged (020) peak, the 2θ peak position of KNN1 was shifted slightly to a higher angle compared with KNN2 nanorods. It could be inferred that the space distances of KNN2 nanorods were a little bigger than KNN1 as calculated by the Bragg's law equation of $n\lambda=2d\sin\theta$, which was in accordance with the HRTEM results. The corresponding ICP of the products shown in Table1 had made a better

explanation about the shift in XRD pattern. The K/Na ratio of KNN2 was 48: 52, indicating more K content and closer to 1 than the 43: 57 of KNN1. The eventually bigger space distances were attributed to the relatively higher K content in KNN2 nanorods, because the radius of K^+ (1.33 Å) was larger than that of Na^+ (0.97 Å)[36], supporting the reason for lower angle in XRD pattern. This phenomenon may be caused by the difference of reaction processes. Both reactions followed a "template formation" mechanism[37]. Na_2CO_3 and K_2CO_3 were much more soluble than the precursors, they would primarily dissolve into the salt, diffuse onto the surfaces of the precursors and react in situ to form the product phase. In this case, the morphologies of the synthesized KNN nanorods would, to a large extent, retain the morphologies of the less-soluble precursors. Using Nb_2O_5 nanorods as precursors, the reaction was considered as in chemical equation (3). The KCl salt transformed to the flux and acted as the solvent where Na_2CO_3 and K_2CO_3 were solutes inside. Na_2CO_3 and K_2CO_3 were needed with the same concentration and diffused on the surfaces of as-synthesized Nb_2O_5 nanorods. But owed to Na reacted more readily with Nb to form $NaNbO_3$ than K for its advantage of ionic radius, Na had a higher reaction activity than K under the same concentration[38]. This was consistent with the results that KNN1 had more Na content. It also indicated that more K source were indispensable in order to obtain the KNN nanorods with expected composition. But the modified composition may not bring much change on the morphology. It's proposed the shortness and agglomeration of KNN1 nanorods originated from the layered structures of the pristine precursors during the synthesis of Nb_2O_5 nanorods. Due to the morphology of Nb_2O_5 nanorods precursors did not change, the morphology of KNN1 with appropriate composition also would not change too much.

However, while using $K_2Nb_4O_{11}$ as precursors, as shown in chemical equation (4), $K_2Nb_4O_{11}$ provided K source and only Na_2CO_3 was needed to provide Na to fill in the A-site for formating KNN solid solution. Na_2CO_3 dissolved into KCl salt, diffused on the surfaces of as-synthesized $K_2Nb_4O_{11}$ nanorods and reacted in situ to form the final product, $K_2Nb_4O_{11}$ nanorods maintained their 1-D morphologyies and K content in the reaction process, resulting in the formation of the KNN2 nanorods with the K/Na ratio

of 48:52,which was closer to the expectation of 50:50.

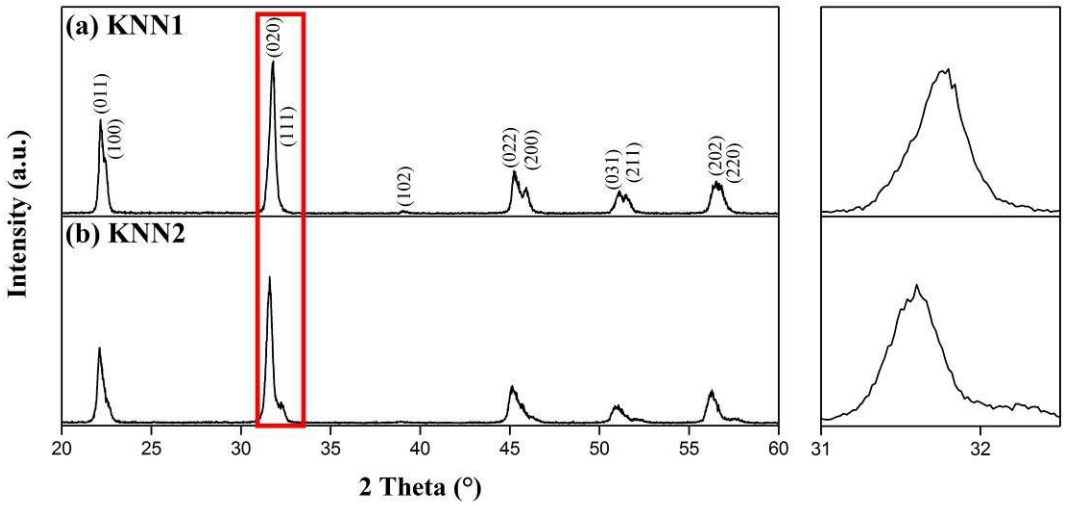

Fig. 9 XRD patterns obtained from (a) KNN1, (b) KNN2, and the expanded XRD patterns conducted in the 2θ range of 31~32.5°.

Table1. The ICP results of the as-synthesized KNN

Sample	K (wt %)	Na (wt %)	K/Na ratio	Formula
KNN1	6.942	5.448	43/57	$(K_{0.43}Na_{0.57})NbO_3$
KNN2	9.315	5.889	48/52	$(K_{0.48}Na_{0.52})NbO_3$

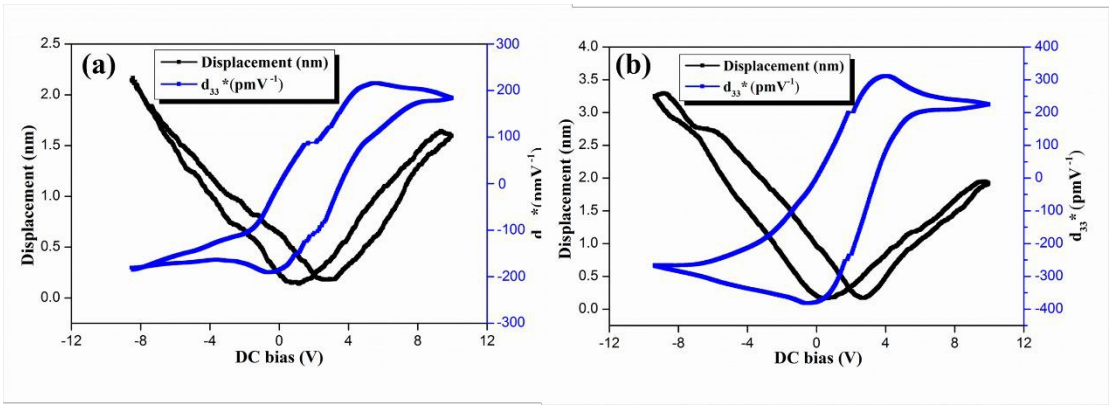

Fig. 10 Displacement–Voltage curve (black line) and calculated d_{33}*–Voltage curve (blue line) obtained from (a) KNN1 nanorod and (b) KNN2 nanorod.

After piezoelectric properties of both KNN nanorods had been tested many times

by PFM, the representative results were shown in Fig. 10. During the test, the DC bias from -10 V to 10 V was applied to the surface of the nanorod, the information of the displacement on the rod was gathered, and the d_{33}* value was calculated by the formula $d_{33}^*=\Delta l/\Delta V$[30]. Fig.10a shows the piezoelectric properties of a randomly selected individual KNN1 nanorod. Typical displacement-voltage 'butterfly' loop was observed with the maximum displacement of 2.21 nm. The 'butterfly' loop was shifted toward a positive voltage, indicating a built-in electric field[39]. The calculated converse piezoelectric coefficient d_{33}* was 95 pm/V. As shown in Fig.10b, the maximum displacement of a randomly selected individual KNN2 nanorod was 3.35 nm. The corresponding d_{33}* of KNN2 nanorods was 201 pm/V. The difference on the piezoelectric properties between both KNN nanorods was consistent with what were discussed above. The K/Na ratio has great influence on piezoelectric properties, a tiny deviation in K/Na ratio away from the 50: 50 can lead to a great decrease in d_{33}[40]. The Na-rich composition in KNN1 was supposed to be the main reason for the decrease of piezoelectric properties as compared with KNN2. The morphologies of KNN nanorods also had influence on the piezoelectric properties. It has been reported that the width of ferroelastic domains was expected to decrease as the nanoscale crystal size reduced, until they disappeared below a critical value[41]. The decrement of the ferroelastic domains for these materials might lead to a reduction to the piezoelectric properties[41]. Therefore, KNN2 nanorods exhibited the preferable morphology, microstructure and piezoelectric properties, which were more suitable for energy harvesting application, as compared with KNN1.

Conclusions

KNN nanorods with a preferred [100] orientation were synthesized by MSS, using Nb_2O_5 and $K_2Nb_4O_{11}$ as precursors, respectively. $K_2Nb_4O_{11}$ nanorods were obtained after the raw materials heated at 1000 °C for 3 h, while Nb_2O_5 was obtained through a series of ion-exchange and thermal decomposition from KNb_3O_8. The final KNN maintained the rod-like morphology of $K_2Nb_4O_{11}$ or Nb_2O_5 precursors. Compared

with the KNN produced by Nb_2O_5 precursors, the one produced by $K_2Nb_4O_{11}$ exhibited much higher aspect ratio of nearly 15:1 and also the separation of particles. Additionally, while using Nb_2O_5 precursors to produce KNN, Na reacted more readily with Nb than K under the same concentration, which resulted in more Na content (the K/Na ratio was 43: 57) than that produced by $K_2Nb_4O_{11}$ precursors (the K/Na ratio was 48: 52). The PFM investigations proved the effects of morphology and composition on piezoelectric properties. The d_{33}* of KNN2 (about 201 pm/V) was much higher than that of KNN1 (about 95 pm/V).

Acknowledgements

This work was financially supported by the Defense Industrial Technology Development Program (Grant no. A1420133028), the National Natural Science Foundation of China (Grant no. 51072235), Hunan Nonferrous Research Funding (Grant no. YSZN2013CL05).

Reference

1. M. Martín-González, O. Caballero-Calero and P. Díaz-Chao, *Renew. Sust. Energ. Rev.*, 2013, **24**, 288-305.
2. G. Wang, S. M. Selbach, Y. Yu, X. Zhang, T. Grande and M.-A. Einarsrud, *CrystEngComm*, 2009, **11**, 1958-1963.
3. Q. Liao, Z. Zhang, X. Zhang, M. Mohr, Y. Zhang and H.-J. Fecht, *Nano Res.*, 2014, **7**, 917-928.
4. Z. L. Wang, *J Nanosci. Nanotechno.*, 2008, **8**, 27-55.
5. P. G. Kang, B. K. Yun, K. D. Sung, T. K. Lee, M. Lee, N. Lee, S. H. Oh, W. Jo, H. J. Seog, C. W. Ahn, I. W. Kim and J. H. Jung, *RSC Advances*, 2014, **4**, 29799.
6. P. M. Rorvik, T. Grande and M. A. Einarsrud, *Adv. Mater.*, 2011, **23**, 4007-4034.
7. L.-Q. Cheng, K. Wang, J.-F. Li, Y. Liu and J. Li, *J Mater. Chem. C*, 2014, 2, 9091-9098.
8. C. Baur, D. J. Apo, D. Maurya, S. Priya and W. Voit, 2014, **1161**, 1-27.
9. C. R. Bowen, J. Taylor, E. LeBoulbar, D. Zabek, A. Chauhan and R. Vaish, *Energy Environ. Sci.*, 2014, **7**, 3836-3856.
10. J. Briscoe and S. Dunn, *Nano Energy*, 2015.
11. S. Saadon and O. Sidek, *Energy Convers. Manage.*, 2011, **52**, 500-504.
12. M. Song, Y. Zhang, M. Peng and J. Zhai, *Nano Energy*, 2014, **6**, 66-72.
13. A. Koka, Z. Zhou and H. A. Sodano, *Energy Environ. Sci.*, 2014, **7**, 288-296.
14. X. Chen, S. Xu, N. Yao and Y. Shi, *Nano Lett.*, 2010, **10**, 2133-2137.

15. X. Chen, J. Li, G. Zhang and Y. Shi, *Adv. Mater.*, 2011, **23**, 3965-3969.
16. H. Luo, D. Zhang, C. Jiang, X. Yuan, C. Chen and K. Zhou, *ACS Appl. Mater. Interfaces*, 2015, **7**, 8061-8069.
17. C. Jiang, K. Zhou, X. Zhou, Z. Li and D. Zhang, *Ceram. Int.*, 2015, **41**, 6858-6862.
18. Z. Fan, H. Lu, B. Shan, S. Tiedong, K. Tomoaki and A. Masatoshi, *Jpn. J. Appl. Phys.*, 2008, **47**, 7685.
19. J. Wu, D. Xiao and J. Zhu, *Chem. Rev.*, 2015.
20. J.-F. Li, K. Wang, F.-Y. Zhu, L.-Q. Cheng, and F.-Z. Yao, *J. Am. Ceram. Soc.*, 2013, **96**, 3677-3696.
21. D.-Q. Zhang, D.-W. Wang, H.-B. Zhu, X.-Y. Yang, R. Lu, B. Wen, W.-Q. Cao, J. Yuan and M.-S. Cao, *Ceram. Int.*, 2013, **39**, 5931-5935.
22. Y. Xu, Q. Yu and J.-F. Li, *J. Mater. Chem.*, 2012, **22**, 23221.
23. Z. Wang, H. Gu, Y. Hu, K. Yang, M. Hu, D. Zhou and J. Guan, *CrystEngComm*, 2010, **12**, 3157-3162.
24. C.-Y. Xu, L. Zhen, R. Yang and Z. L. Wang, *J. Am. Chem. Soc.*, 2007, **129**, 15444-15445.
25. K. H. Yoon, Y. S. Cho and D. H. Kang, *J. Mater. Sci.*, 1998, **33**, 2977-2984.
26. L.-Q. Cheng, K. Wang and J.-F. Li, *Mater. Lett.*, 2015, **138**, 128-131.
27. L. Li, J. Deng, R. Yu, J. Chen, X. Wang and X. Xing, *Inorg. Chem.*, 2010, **49**, 1397-1403.
28. L. Li, J. Deng, J. Chen, X. Sun, R. Yu, G. Liu and X. Xing, *Chem. Mater.*, 2009, **21**, 1207-1213.
29. F. Madaro, J. R. Tolchard, Y. Yu, M.-A. Einarsrud and T. Grande, *CrystEngComm*, 2011, **13**, 1350-1359.
30. L. Q. Cheng, K. Wang and J. F. Li, *Chem. Commun.*, 2013, **49**, 4003-4005.
31. R. Nedjar, M. M. Borel and B. Raveau, *Mater. Res. Bull.*, 1985, **20**, 1291-1296.
32. M. A. Bizeto and V. R. L. Constantino, *Mater. Res. Bull.*, 2004, **39**, 1729-1736.
33. S. Xu and J.-F. Li, *J. Am. Ceram. Soc.*, 2011, **94**, 3812-3818.
34. L.-Q. Cheng, K. Wang, Q. Yu and J.-F. Li, *J Mater. Chem. C*, 2014, **2**, 1519.
35. F. Madaro, R. Sæterli, J. R. Tolchard, M.-A. Einarsrud, R. Holmestad and T. Grande, *CrystEngComm*, 2011, **13**, 1304-1331.
36. X. Pang, J. Qiu, K. Zhu and J. Du, *Ceram. Int.*, 2012, **38**, 2521-2527.
37. Z. Cai, X. Xing, R. Yu, X. Sun and G. Liu, *Inorg. Chem.*, 2007, **46**, 7423-7427.
38. L. Su, K. Zhu, J. Qiu and H. Ji, *J. Mater. Sci.*, 2010, **45**, 3311-3317.
39. M. Cernea, L. Trupina, C. Dragoi, B. S. Vasile and R. Trusca, *J. Alloys Compd.*, 2012, **515**, 166-170.
40. B.-P. Zhang, J.-F. Li, K. Wang and H. Zhang, *J. Am. Ceram. Soc.*, 2006, **89**, 1605-1609.
41. N. Salazar, M. Algueró, H. Amorín, A. Castro, A. Gil and J. Ricote, *J. Appl. Phys.*, 2014, **116**, 124108.